Neural, Parallel, and Scientific Computations 21 (2013) 319-334

QUANTITATIVE ULTRASOUND-MODULATED OPTICAL TOMOGRAPHY: A DIRECT GAUSS-NEWTON APPROACH TO RECOVER ELASTICITY DISTRIBUTION FROM THE MEASURED INTENSITY AUTOCORRELATION

K. P. MOHANAN, A. K. NANDAKUMARAN, D. ROY, AND RAM MOHAN VASU

Department of Instrumentation and Applied Physics
IISc, Bangalore-560012, India
Department of Mathematics, IISc, Bangalore-560012, India
Department of Civil Engineering, IISc, Bangalore-560012, India
Department of Instrumentation and Applied Physics
IISc, Bangalore-560012, India

ABSTRACT. We demonstrate a direct recovery of elasticity distribution from ultrasound-modulated optical tomography data gathered at a single detector. The reconstructions are seen to be of good quality and the convergence of the algorithm quick. We have en route devised a means to estimate the Jacobian needed for this reconstructions which uses both the equations of correlation transport and momentum balance. The inversion scheme uses the Gauss-Newton algorithm resulting in a fast decay of the error to convergence in less than 10 iterations in most of the cases.

AMS (MOS) Subject Classification: 35J25, 35Q60, 78A70

1. Introduction

Ultrasound-modulated optical tomography (UMOT) [1], [2] has been introduced as a remedy for the poor resolution in the optical contrast recovery available from diffuse optical tomography (DOT). In UMOT, a tightly focused ultrasound (US) beam introduces mechanical vibration in a localized region presently referred to as the region of interest (ROI) in the object to be imaged, thereby resulting in a modulation of the refractive index ($n(\mathbf{r})$) and the mean position of the scattering centers [3]. A coherent light beam interrogating the object picks up a phase modulation from the insonified ROI, which is reflected as a modulation in the amplitude autocorrelation ($G(\mathbf{r},\tau)$) of light. What is usually measured is the intensity autocorrelation $g_2(\mathbf{r},\tau) = \langle I(\mathbf{r},\tau)I(\mathbf{r},t+\tau)\rangle$ a quantity that is related to $g_1(\mathbf{r},\tau) = G(\mathbf{r},\tau)/G(\mathbf{r},0)$ through the Seigert relation [4] from which optical and mechanical properties of the material in ROI can be reconstructed. The mechanical property is the Young's modulus influencing the amplitude of oscillation of the scattering centers. In an earlier work, we have demonstrated the recovery of $p(\mathbf{r})$, the distribution of the mean-squared

Received July 15, 2013

amplitude of vibration (i.e. $p(\mathbf{r}) = \langle |A(\mathbf{r})|^2 \rangle$, where $\langle\rangle$ represents averaging the amplitude $A(\mathbf{r})$, over a volume $(l^*)^3$, with l^* denoting the transport-mean-free path) from M, the modulation depth in $g_1(\mathbf{r}, \tau)$ measured (or inferred) at the boundary. Since local absorption coefficient $\mu_a(\mathbf{r})$, together with $p(\mathbf{r})$ and $n(\mathbf{r})$ influence M, it should be possible, at least in theory, to recover all the above three parameters pertaining to the ROI from a set of M measured on the boundary. In [2], we have demonstrated the recovery of $p(\mathbf{r})$ distribution (space-resolved tomographic recovery) in the ROI. For this, a perturbation equation was set up from the correlation diffusion equation (CDE) describing propagation of $G(\mathbf{r}, \tau)$ in a turbid medium, in order to relate the US induced perturbations in the ROI (which are in $n(\mathbf{r})$ and the dynamics of the scattering centers) to M which is related to the perturbation on $G(\mathbf{r}, \tau)$. This equation, which provides a nonlinear relationship between $p(\mathbf{r})$ and M (as in [2]), is solved either directly, using an iterative procedure, or, for ease of computation, after linearization at $p = 0$. The solution involves an error minimization strategy (i.e. find $p(\mathbf{r})$ which minimizes $\varepsilon(p) = \frac{1}{2}|M^e - M^c|^2$ where M^e is the experimentally measured modulation length and M^c is its computationally obtained counterpart) and employs an iterative regularized Gauss-Newton algorithm. In [2] recovery of $p(\mathbf{r})$ within the ROI, typically the region of inhomogeneous Youngs modulus distribution, had a spatial resolution limited to l^* owing to the diffusion model used for modeling the propagation of $G(\mathbf{r}, \tau)$.

The novelty of this paper is in the form of a single direct recovery of Young's modulus from M^e without recovering $p(\mathbf{r})$. This requires an additional partial differential equation (PDE), a momentum balance equation connecting $A(\mathbf{r})$ to the Young's modulus distribution and the external sinusoidal forcing applied. The $A(\mathbf{r})$ is tied to the measurement M through the PDE that $G(\mathbf{r}, \tau)$ obeys which contains $p(\mathbf{r})$ as a parameter. The second PDE is viewed as a constraint that $A(\mathbf{r})$ (from which $p(\mathbf{r})$ is computed) should satisfy. The two PDEs help to compute the measurement M given a distribution of Young's modulus (E) and Poissons ratio. In addition, with their help, we also compute the Jacobian matrix giving the rate of change of M to E as the composite of the Jacobians of M with respect to p and p with respect to E, where we also employ a measurement operator connecting A to p. The nonlinear relation which connects M to E is locally linearized and the perturbation equation connecting changes in M to changes in E is setup and inverted for update in E. The local linearization of $M(E)$ is redone at the new $E(\mathbf{r})$ and a new update for $E(\mathbf{r})$ is obtained.

In this work, another novel modification is introduced to greatly simplify the data collection experiment. Since the modulation depth is to be obtained with good signal-to-noise ratio the interface to the photo-detector is through a single-mode fiber which is painstakingly aligned to a single speckle. To have sufficient data in a tomography

experiment a multitude of detectors are used for each source location which would make the alignment (and its maintenance) very cumbersome. In diffuse optical tomography (DOT)which aims to recover functional parameters such as oxygen partial pressure and concentration of hemoglobin and lipids from recovered spectroscopic variation of absorption coefficient (μ_a) data collection is simplified by substituting many detectors with only a few whilst making up for the loss of data by scanning over wavelengths (λ) of importance [5], [6]. Sure enough as λ varies the number of unknowns to be recovered (μ_a) also increases making the inversion more ill-posed. One way to address this difficulty could be by projecting the increasing set of μ_a to a new set of unknowns which are the concentration of functional parameters that are λ-invariant. Specifically, in the present work, a simplification is effected by replacing the data over many locations by those corresponding to variation over acoustic frequency. Similar to the DOT there is an increase in the dimension of the primary unknown which is the discretized set obtained from $p(\mathbf{r})$; but here we escape this growth and the consequent instability in the reconstruction through projecting $p(\mathbf{r})$ to $E(\mathbf{r})$ (the latter being invariant to acoustic frequency) through a momentum balance equation as applied to the vibrating ROI. The experimental simplification achieved, as seen in Section 4 below, is that we can get enough orthogonal data with barely one (or at most two) detectors.

The rest of the paper is organized as follows. In Section 2, the forward models, connecting the measurement, first to the amplitude of vibration, and then to Young's modulus, are introduced. In Section 3, the inverse problem of recovering $E(\mathbf{r})$ from the measurement is posed as one of error minimization and solved through a regularized Gauss-Newton algorithm. Here the computation of the Jacobian matrix making use of the forward PDEs is also described. Numerical simulations demonstrating the efficacy of the procedure are given in Section 4. The concluding remarks are in Section 5.

2. Forward models for correlation propagation and momentum balance

2.1. **A model used for correlation diffusion in a turbid medium.** It has been shown [3] that the specific intensity $I(\mathbf{r}, \hat{k}_s, \tau)$ at a point $\mathbf{r}$ and time τ in the direction given by the unit vector $\hat{k}_s$ obeys a correlation transport equation (CTE). In a medium where scattering predominates, an angle-averaged version of $I(\mathbf{r}, \hat{k}_s, \tau)$, given by $G(\mathbf{r}, \tau) = \int_{4\pi} I(\mathbf{r}, \hat{k}_s, \tau) d\hat{k}_s$ and referred to as the amplitude autocorrelation, obeys the following diffusion equation:

$$-\nabla \cdot \kappa \nabla G(\mathbf{r}, \tau) + (\mu_a + 2\mu_s k_0^2 D_B \tau) G(\mathbf{r}, \tau) = S_0(\mathbf{r}_0) \tag{2.1}$$

Here $\kappa = \frac{1}{3(\mu_a + \mu_s')}$ is the optical diffusion coefficient, where μ_a and μ_s' are the optical absorption and (reduced) scattering coefficients respectively. Moreover D_B is the particle diffusion coefficient of the medium, k_0 is the modulus of the light propagation

vector and S_0 is the strength of the isotropic point source at $\mathbf{r}_0$. The term $2\mu_s k_0^2 D_B \tau$ is owing to the Brownian motion of the scattering centers induced by the background temperature. When a focused US beam insonifies the object, it produces a refractive index modulation (Δn) and oscillations in the scattering centers in the focal region, the ROI, which is approximately hyperboloidal in shape whose volume and length-to-width ratio can be tailored by the parameters such as the focal length and $f/$ No. of the focusing US transducers [7]. At this stage, we neglect the modulation Δn and consider the oscillations introducing a perturbation term in Eq. (2.1) which, in turn, perturbs $G(\mathbf{r},\tau)$ to $G(\mathbf{r},\tau)+G^\delta(\mathbf{r},\tau)$. The equation (2.1) thus becomes:

$$-\nabla\cdot\kappa\nabla(G+G^\delta)(\mathbf{r},\tau)+(\mu_a+B(\mathbf{r},\tau)+A(\tau)\chi_I p(\mathbf{r},\tau))(G+G^\delta)(\mathbf{r},\tau)=S_0(\mathbf{r}_0) \tag{2.2}$$

Here the perturbation term on the left-hand side is denoted by $A(\tau)\chi_I p(\mathbf{r},\tau)$ where $A(\tau)=c\sin^2\frac{\omega_a\tau}{2}$ and χ_I is the characteristic function over I, the insonified ROI. Further, ω_a is the acoustic frequency in radians and c is a constant depending on l^*, k_a, the acoustic wave vector and the elasto-optic coefficient of the material of the object [3]. Equation (2.2) is supplemented with the boundary condition:

$$(G+G^\delta)(\mathbf{r},\tau)+\kappa\frac{\partial(G+G^\delta)(\mathbf{r},\tau)}{\partial n}=0,\ \mathbf{r}\in\partial\Omega \tag{2.3}$$

The equation (2.1) is also given the Robin-type boundary conditions. Given all the material properties, and the US-induced oscillations, Eqs. (2.2) and (2.3) can be solved to get $(G+G^\delta)(\mathbf{r},\tau)$ which is the forward solution of UMOT. This facilitates computing a quantity M, which is the measurement in UMOT given by:

$$M(p,\mathbf{r},\omega)=\left|\int_0^\alpha (G+G^\delta)(\mathbf{r},\tau)\exp^{-j\omega\tau}\,d\tau\right|_{\omega=\omega_a} \tag{2.4}$$

Here, ω_a is also the frequency of the US forcing. Yet another related measurement is obtained from $G^\delta(\mathbf{r},\tau)$ that is readily computable from the perturbation equations (2.6) and (2.7) (to be given below):

$$M_1(p,\mathbf{r},\omega_a)|_{\mathbf{r}\in\partial\Omega}=\left|\int_0^\alpha G^\delta(\mathbf{r},\tau)\exp^{-j\omega\tau}\,d\tau\right|_{\omega=\omega_a}. \tag{2.5}$$

In an experiment, intensity autocorrelation is measured, from which $M(p,\mathbf{r},\omega)$ is easily computed; however, M_1 is easily obtained from M by subtracting the background pedestal from M at $\omega=\omega_a$. With this measurement, (a part of) the inverse problem of UMOT is the recovery of $p(\mathbf{r})$ given $M_1(p,\mathbf{r},\omega_a)$ and the forward model of Eqs. (2.2) and (2.3). In order to facilitate this inversion, we first rewrite the forward equation as a perturbation equation given by

$$-\nabla\cdot\kappa\nabla G^\delta(\mathbf{r},\tau)+(\mu_a+B(\mathbf{r},\tau)+A(\tau)\chi_I p(\mathbf{r},\tau))G^\delta(\mathbf{r},\tau)=-A(\tau)\chi_I p(\mathbf{r},\tau)G(\mathbf{r},\tau) \tag{2.6}$$

with the boundary condition

$$G^{\delta}(\mathbf{r},\tau)+\kappa\frac{\partial G^{\delta}(\mathbf{r},\tau)}{\partial n}=0,\ \mathbf{r}\in\partial\Omega \tag{2.7}$$

The above equation connects $p(\mathbf{r},\tau)$ nonlinearly to $G^{\delta}(\mathbf{r},\tau)$ because of the presence of a term containing $p(\mathbf{r},\tau)$ on the left-hand side (LHS) of it. If we neglect the term containing the product of G^{δ} and p from the LHS of Eq. (2.6), then it becomes linear in the unknown p and hence renders computationally more expedient the inversion of p using equations (2.6) and (2.7). When we use the linearized perturbation equation given by

$$\nabla\cdot\kappa\nabla G^{\delta}(\mathbf{r},\tau)-(\mu_a+B(\mathbf{r},\tau))G^{\delta}(\mathbf{r},\tau)=A(\tau)\chi_I p(\mathbf{r},\tau)G(\mathbf{r},\tau), \tag{2.8}$$

the following simplifications in the computations accrue [2]. For example, the derivatives need not be re-estimated during the course of the algorithm, but only $(F(p^i)-M^e)$. Also the structure of the partial differential equation (PDE) part of the Frchet derivative operator retains the structure of the forward propagation PDE (Eq. (2.1)) and therefore, *en route* to recovery of $p(\mathbf{r})$, (when one desires only a recovery of $p(\mathbf{r})$) for the calculation of the Jacobian one need only solve the adjoint of Eq. (2.1). The FEM discretization of PDE (2.8) leads to a set of linear algebraic equations represented by:

$$\mathbf{K}(p)G^{\delta}=\mathbf{q} \tag{2.9}$$

where $\mathbf{K}(p)$ is the system matrix and $\mathbf{q}$ is the source vector. As indicated earlier, we have used this equation derived from the linearized version of the perturbation equation (Eq. (2.8)) in our inversion scheme. In accordance with the simplified data collection strategy, we sweep the US frequency resulting in a set of $p(\mathbf{r})$'s for a given $E(\mathbf{r})$. To compute the data M_1 we use these $p(\mathbf{r})$'s in Eqs. (2.8) and (2.5).

2.2. **The momentum balance equation.** Here the object under consideration is only a part of the one considered in Section 2.1, the portion insonified by the focusing ultrasound (US) transducer where the displacement is nonzero, designated earlier the (ROI), Ω_f. In contrast, the focal region is defined to be the support of the US transducer-induced radiation force. To find Ω_f, we first compute the US force [8] corresponding to an approximated focal region (e.g. by incorporating the nodes where the force exceeds a small fraction of its maximum in a central node) and then solve for displacement via the momentum balance equation for the entire object, now considered an infinite medium vis-a-vis the focal region. The internal Dirichlet boundary $\partial\Omega_f$ thus separates the zero-displacement region of the object from the rest.

Towards computing the displacement field via an inversion of the momentum balance equation, a plane stress approach based on a 2D linear elasticity setup is adopted,

with the ROI material being assumed to be nearly incompressible. Under strictly sinusoidal US forcing and the linear elasticity framework, the vibrating ROI would exhibit sinusoidal response with the frequency of the excitation once the transients die out. Accordingly, the so called mixed form of the governing equations (in terms of the amplitude $\mathbf{u}_0(\mathbf{r})$ of the displacement vector field $u(\mathbf{r},t) := (\mathbf{u}(\mathbf{r},t), q(\mathbf{r},t))^T$ and the pressure field $q(\mathbf{r})$ takes the form [9]:

$$\rho\omega^2\mathbf{u}_0 + \nabla\cdot\left(-q\mathbf{I} + \frac{E}{2(1+\nu)}(\nabla\mathbf{u}_0 + (\nabla\mathbf{u}_0)^T)\right) = f_0;\ \mathbf{r}\in\Omega_f \tag{2.10a}$$

$$\nabla\cdot\mathbf{u}_0 = -\frac{q(1+\nu)(1-2\nu)}{E\nu};\ \mathbf{r}\in\Omega_f \tag{2.10b}$$

with only the Dirichlet boundary condition:

$$\mathbf{u}_0 = 0 \text{ for } \mathbf{r}\in\partial\Omega_f \tag{2.10c}$$

Here E denotes Young's modulus, ν Poissons ratio, ρ material density, $\mathbf{f}_0(\mathbf{r})$ the forcing amplitude vector and q the pressure, all referred to the undeformed configuration. Finally, ω denotes the US forcing frequency. In the context of the FEM, Eq. (2.10) may be successfully solved via a mixed weak formulation even as the material approaches the incompressibility limit (i.e. as $\nu\to 0.5$). The problem involved in the weak formulation is to find $u = (\mathbf{u}_0, q)\in H^1(\Omega_f)\times L^2(\Omega_f)/\mathbb{R}$ so as to satisfy:

$$B(\boldsymbol{w}, u) = (\mathbf{w}, \mathbf{f}_0),\ \forall\ \boldsymbol{w} = (\mathbf{w},\varphi)\in H_0^1(\Omega_f)\times L^2(\Omega_f) \tag{2.11a}$$

Here $(\mathbf{w},\mathbf{f}_0) = \displaystyle\int_{\Omega_f}\mathbf{w}\cdot\mathbf{f}_0 d\Omega_f$ is the linear form and $B(\boldsymbol{w},u)$ the bilinear form defined as:

$$\begin{aligned} B(\boldsymbol{w},u) = &\int_{\Omega_f}\left(\rho\omega^2\mathbf{w}\cdot\mathbf{u}_0 - \left[\nabla\mathbf{w}+\nabla\mathbf{w}^T\right] : \left[\frac{E}{4(1+\nu)}\left(\nabla\mathbf{u}_0 + (\nabla\mathbf{u}_0)^T\right)\right]\right)d\Omega_f \\ &+\int_{\Omega_f}\left((\nabla\cdot\mathbf{w})q + \varphi\nabla\cdot\mathbf{u}_0 + \frac{\varphi q}{\beta E}\right)d\Omega_f, \end{aligned}$$

where β is a large scalar multiplier ensuring that the bulk modulus is much higher than E.

Indeed the pressure q can be eliminated using the second equation in (2.10) and one can get a weak formulation for $\mathbf{u}_0$ alone. In the FE implementation, the equation (2.11) may finally be reduced to the matrix-vector equation given by:

$$K^h u^h = \mathbf{s}^h \tag{2.12}$$

where h denotes the characteristic element size, K^h the so-called stiffness matrix, u^h the unknown vector (in general consisting of both the nodal displacement amplitudes and pressure) and s^h the source vector Equation (2.12) is inverted for u^h and $p(\mathbf{r}) = \langle|u^h(\mathbf{r})|^2\rangle$.

3. Direct recovery of E from modulation depth

We introduce the operator $\mathcal{F}_1(\mu_a, p, \kappa) = G^\delta$ through Eq. (2.8) and the measurement operator $\mathcal{M}_1(G^\delta) = M_1$ through Eq. (2.5). Then the composite operator $\mathcal{F}_A = \mathcal{M}_1 \odot \mathcal{F}_1$ maps p to $\mathcal{M}_1$. Similarly, we introduce $\mathcal{F}_2(E, \rho, \nu) = \mathbf{u}$ using Eq. (2.10), the measurement operator $\mathcal{M}_2(\mathbf{u}) = p$ through $p(\mathbf{r}) = \langle |u(\mathbf{r})|^2 \rangle$ and the composite operator $\mathcal{F}_B = \mathcal{M}_2 \odot \mathcal{F}_2$ which maps E to $p(\mathbf{r})$. With these, we define the operator, $\mathcal{F} = \mathcal{F}_A \odot \mathcal{F}_B$ which maps E to M_1, the measurement from the UMOT experiment. Our attempt is to recover E from M_1 through the (direct) inversion of $\mathcal{F}$.

3.1. Parameter estimation through nonlinear optimization.

We invert the equation $\mathcal{F}(E) = M_1$ for E_1 by solving the following nonlinear minimization problem:

$$\underset{E \in L^\infty(\Omega_f)}{\text{Minimize}}\ \Theta(E) = \frac{1}{2}\|\mathcal{F}(E) - M_1\|^2_{L^2(\partial\Omega_f)} + \frac{\lambda}{2}\|E\|^2_{L^2(\Omega_f)} \tag{3.1}$$

Here λ is an appropriate regularization parameter. We employ the Gauss-Newton algorithm to arrive at this minimization through the iteration

$$E^{i+1} = E^i - H(E^i)^{-1} G(E^i) \tag{3.2}$$

where H and G are the Hessian and Gradient of error functional Θ evaluated at $E = E^i$ using

$$H(E)(\delta E) = (D\mathcal{F}^*(E) D\mathcal{F}(E) + \lambda I)(\delta E) \text{ and } G(E) = D\mathcal{F}^*(\mathcal{F}(E) - M_1), \tag{3.3}$$

where I denotes the identity matrix, (δE) is an increment in E and $D\mathcal{F}$ and $D\mathcal{F}^*$ are the Frechet derivative and its adjoint of $\mathcal{F}$. The Frechet derivative, or more appropriately its finite dimensional equivalent, the Jcobian, is a matrix whose elements are the rate of change of measurement(s) with respect to nodal values of E. This is obtained by combining the derivatives of M_1 with respect to $\mathbf{p}$ (which is the discretized version of $p(\mathbf{r})$) and those of E with respect to $\mathbf{p}$.

For the correlation propagation equation we have derivatives of the type $\frac{\partial M_{1i}}{\partial p_j}$, the computation of which should involve two forward solves of the correlation diffusion equation (CDE). A complete row of the Jacobian matrix can be computed with only one forward solve of the CDE and its adjoint, making use of the reciprocity relation which light diffusion obeys [2]. Similarly, for $\frac{\partial p_i}{\partial E_j}$ the momentum-balance equation (Eq. (2.10)) and its adjoint as given in [9], can be made use of. However, since the number of unknowns in Ω_f and the number of measurements ($\mathbf{p}$) are equal the computational advantage of using the adjoint formulation is little; therefore for this part we use the perturbation scheme which involves two forward solves for each nodal unknown.

In order to compute a typical element of the Jacobian matrix $J = \left\{ \frac{\partial M_{1i}}{\partial E_j} \right\}$ one should consider the fact that a change in E at a typical node, δE_j, necessarily results in changes of $\mathbf{p}$ at all nodes. Therefore, $\frac{\partial M_{1i}}{\partial E_j} = \sum_{k=1}^{N} \frac{\partial M_{1i}}{\partial p_k} \frac{\partial p_k}{\partial E_j}$; the evaluation of this requires all the N derivatives of the type $\frac{\partial p_k}{\partial E_j}$. The set of all derivatives is evaluated using the appropriate forward equation (Eqs. (2.6), (2.7) and (2.11)).

Once the derivatives are computed, Eq. (3.2) is set-up and the increment in E, $(\delta E)^i$ is obtained from it. A direct inversion of $H(E^i)$ is not attempted; instead a second optimization step using a conjugate gradient search to reach the optimal point is employed. The algorithm is stopped when the norm of the error between experimental measurement and its computed counterpart becomes below a preset small value.

4. **Numerical simulations**

We consider two objects, both 2-D, one a rectangular cross-section of a slab and the other a circular cross-section of a cylinder. (We note that a plane stress approximation is not necessarily valid for any cross-section of the insonified volume which receives the US forcing. However, to demonstrate recovery of the location and approximate validation of quantitative variation of E in a computationally expedient manner, we chose a 2-D problem.) The object is assumed to have acoustic and optical properties to match those of (poly) vinyl alcohol (PVA) gel which have gone through two cycles of freezing and thawing [10]. The dimensions of the objects are 6cmx4cm (for the rectangular one) and 6cm diameter (for the circular one). The optical properties are: μ_a (absorption coefficient) = 0.1 cm^{-1} and μ_s'(reduced scattering coefficient) = 8.0 cm^{-1}. The mechanical properties are: E (Background Young's modulus) = 11300 Pa, ρ (density)=1 cgs unit and ν (Poisson's ratio)=0.49.

We locate the origin of co-ordinates at the centre of the object domain. With this, for parallel illumination from a laser, the equivalent isotropic source is at one l^* inside the boundary point where the parallel beam strikes the object, which is assumed at (-2.875,0.0). (Note: Unit of length is cm everywhere.) A confocal US transducer with two regions oscillating at f and $f + \delta f$ Hz focuses its beams to a region in Ω (the ROI) assumed hyperboloidal with centre at (2.0,0.0). The waves mix in the ROI and produce a difference frequency forcing at (δf) Hz. It is this frequency difference we vary in the simulations to gather a number of modulation depth measurements. In our simulations f is chosen to be 1 MHz. The hyperboloidal shape is verified by solving the Westervelt equation [8] for acoustic pressure propagation through the object and computing the distribution of force in the focal region, which is shown in Fig. 1. The size of the ROI is found to be of length 1.42 cm and width of the waist

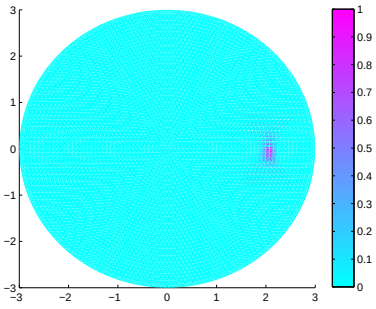

FIGURE 1. Computed distribution of force in the focal region of the US transducer

region 0.2 cm. The interrogating light beam is either sent along the US transducer axis or perpendicular to it.

When the momentum-balance equation is solved with the beat frequency of the two-region US transducer incremented from low (from around 300 Hz in our case) to high frequency (to nearly 600 Hz in our case) we observe that the amplitude of vibration goes through many resonant peaks. The δf scan in our numerical simulations is so chosen to cover the sharply varying regions around the three resonant peaks in the frequency response.

In the ROI, inhomogeneities are introduced in Young's modulus. In the first case, the central region has a higher E of 22.39 KPa and the peripheral upper and lower regions have an E the same as that of the background which is 11.3 KPa (see Figs. 2(a) and 6(a)). In the second case, the inhomogenous regions are at top and bottom of the ROI with $E = 22.39$ KPa and the central region has E at the background level of 11.3 KPa (see Figs. 6 and 14).

The rectangular object is discretized with a Finite Element (FE) mesh with 13168 triangular elements and 6740 nodes. For the circular object these values are 14976 and 7633 respectively. As indicated earlier, we have used just a single light source and detector and the modulation depth in the amplitude autocorrelation (M_1) is computed by solving Eqs. (2.8) and (2.5). The $p(\mathbf{r})$ used in Eq. (2.8) is obtained by solving Eq. (2.10); a set of 50 measurements $\{M_1\}$ is generated by employing $p(\mathbf{r})$'s generated by varying the US frequency used in Eq. (2.10). The 'experimental' measurement is obtained from M_1 by adding an 1% noise.

The sets of measurements generated with the two objects are input a Gauss-Newton algorithm [2] to recover E. The increments for δE are obtained by inverting the linearized perturbation equation (Eq. (3.2)) which is the heart of the Gauss-Newton procedure. The δE updates the elasticity vector and the perturbation equation itself is updated with the help of the two forward equations, Eqs. (2.8) and (2.10).

The value of the regularization parameter used in the algorithm (λ) at the start is 3.2116×10^{-54}, which is reduced by a factor of 1.5 at each iteration.

4.1. **Results and discussions.** The data (M_1) gathered from the rectangular objects shown in Figs. 2(A) and 2(B), are input to the Gauss-Newton algorithm and the gray-scale images of the reconstruction of the isonified ROI are in Figs. 3(A) and 3(B). The cross-sectional plots through the original object and the reconstruction are shown in Fig. 4(A) (for case (i) with central δE inhogeneity) and Fig. 4(B) (for case(ii) with δE inhomogeneity at the peripheries). The decay of the error measured in the data domain is shown in Figs. 5(B) and 5(B) for the two cases.

The circular disc objects with inhomogeneous inclusions are shown in Figs. 6(A) and 6(B) and their reconstructions are in Figs. 7(A) and 7(B). The cross-sectional plots through the centre of the inclusion are in Figs. 8(A) and 8(B) (for the two cases) and data-domain error .vsiteration number in Figs. 9(A) and 9(B).

It is seen form the reconstructions and the error plots that the new procedure is able to recover the Young's modulus distribution from correlation modulation measurements from a single detector. The absence of data from many detectors is compensated by that at many US frequencies. Excepting for the case of circular object with inhomogeneity at the periphery of the ROI for all the others the algorithm converged in 5–6 iterations and for the case mentioned it took 18–19 iterations. We have thus shown that the data gathered here with US frequency are linearly independent and can be used for tomographic inversion of a parameter like E which is invariant to change in US frequency. The goal of the present work is also to introduce a scheme which is experimentally viable. (Correlation modulation measurement with a large number of detectors is quite cumbersome for experimental implementation). The experiment set-up is currently under development and the results from this will be the subject of another publication.

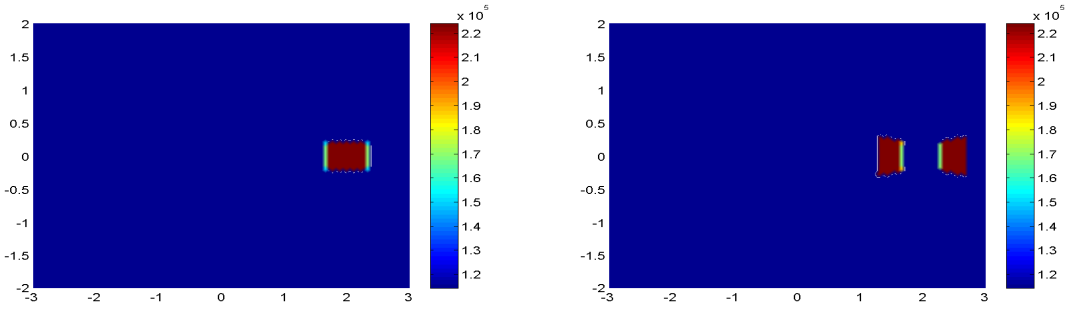

(A) (B)

FIGURE 2. The grey-scale image of the rectangular object with inhomogeniety in E at the US focal region. (A) the central area has larger E value and (B) peripheral area has larger E value. The unit of E is in KPa.

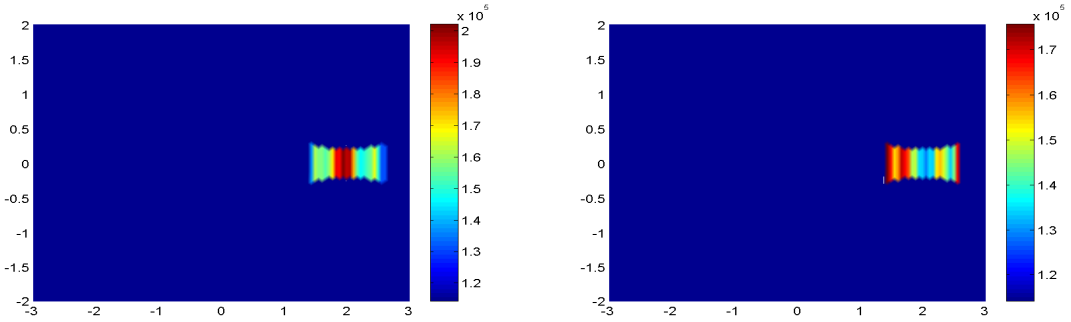

(A) (B)

FIGURE 3. Reconstructed images corresponding to the originals in Figures 2(A) and 2(B), respectively. The unit of E is in KPa.

5. **Conclusions**

We have devised a new scheme to recover Young's modulus from UMOT data which gathers data using only a single detector, but at many US frequencies. When the US frequency varies the oscillation amplitude introduced by the US force also varies. Therefore, an algorithm which aims to recover $p(\mathbf{r})$ which is related to this amplitude will not succeed here because of ill-conditioning of the inversion scheme arising out of the large dimension of the unknown vector. However, when we project $p(\mathbf{r})$ to E which does not vary with frequency, the problem with the present data set becomes well-posed. We have used numerically simulated data and shown the reconstruction results showing space-resolved elasticity map within the US focal region. We note that light diffusion puts a resolution limit to the recovery depending on l^*. Within this limitation we have shown that a tomographic recovery of the distribution of elasticity is possible from data gathered at a single detector.

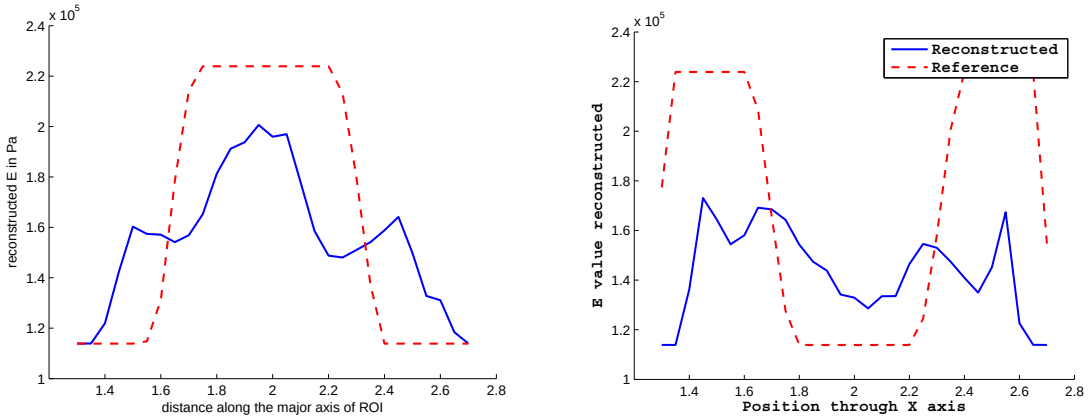

(A) (B)

FIGURE 4. Cross-sectional plots through the center of the reconstructed inhomogenity (shown in Figure 3) compared with that for the original.

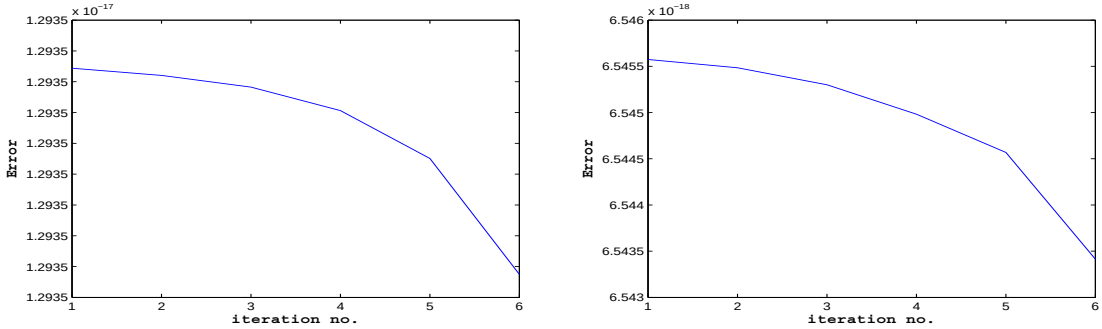

(A) (B)

FIGURE 5. Data domain mean-square error .vs. iteration number corresponding to the reconstruction shown in Figures 3(A) and 3(B)

ACKNOWLEDGMENTS

A. K. Nandakumaran and R. M. Vasu were partially supported by the Council of Scientific and Industrial Research under the project No.25(D194)/11/ EMR-II dated 02/02/2011. A. K. Nandakumaran would also like to thank UGC for the support to the Center for Advanced Studies, Department of Mathematics, IISc.

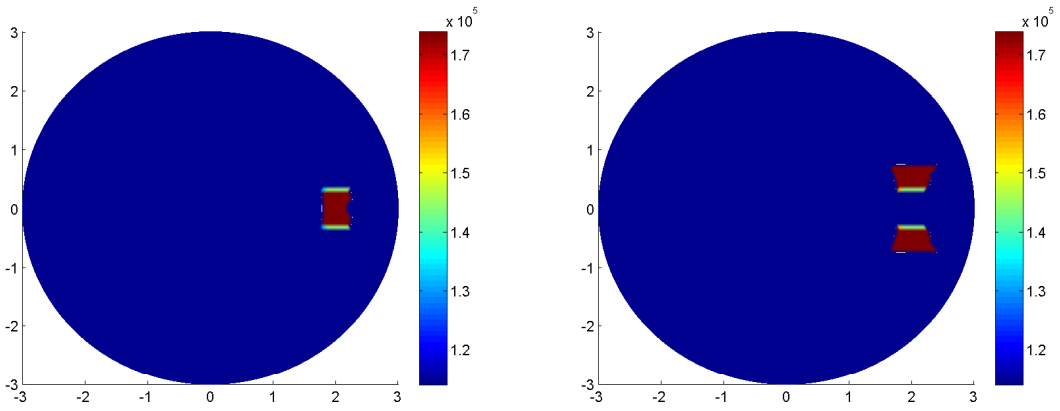

(A) (B)

FIGURE 6. The grey-scale image of the circular object with inhomogeneity in E at the US focal region. (A) the central area has larger E value and (B) peripheral area has larger E value. The unit of E is in KPa.

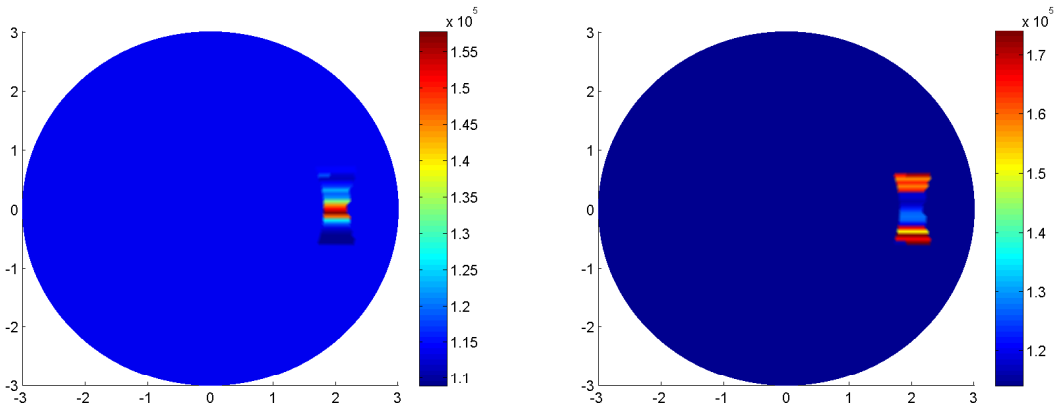

(A) (B)

FIGURE 7. Reconstructed images corresponding to the originals in Figures 6(A) and 6(B), respectively. The unit of E is in KPa.

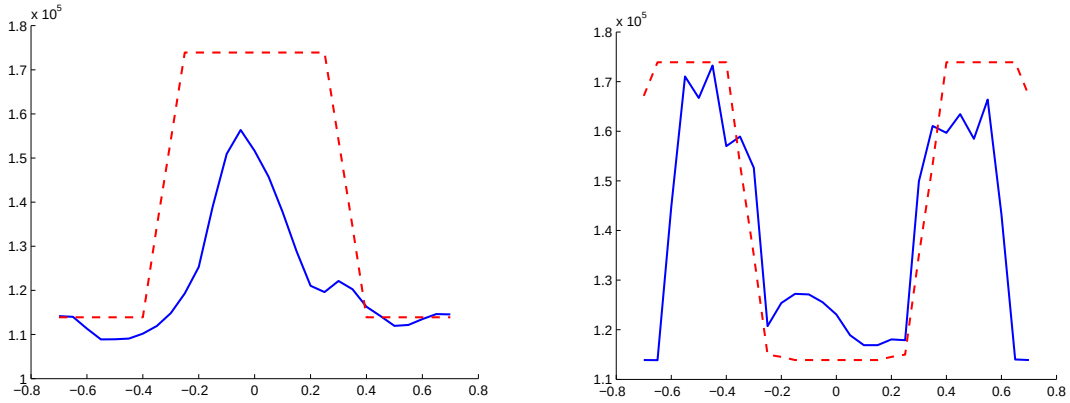

(A) (B)

FIGURE 8. Cross-sectional plots through the center of the reconstructed inhomogeneity (shown in Figure 7) compared with that for the original.

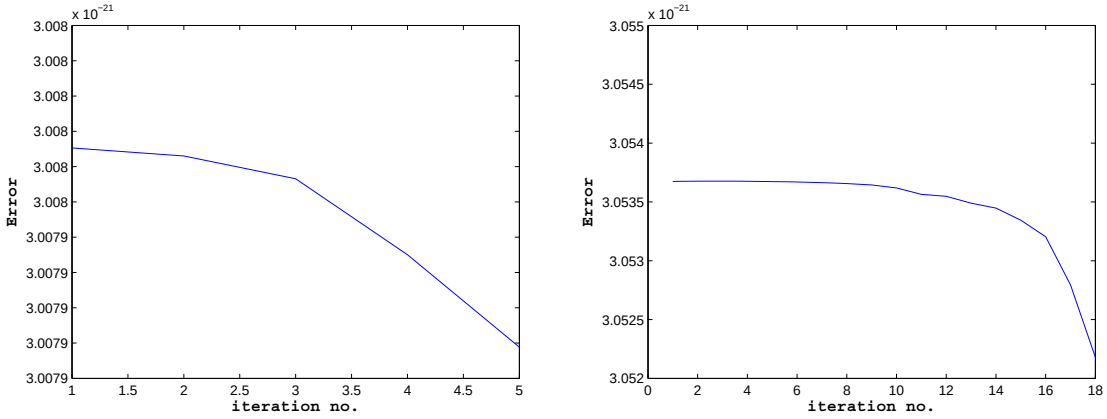

(A) (B)

FIGURE 9. Data domain mean-square error .vs. iteration number corresponding to the reconstruction shown in Figures 7(A) and 7(B).

REFERENCES

[1] S. Gupta, H. M. Verma, N. Hynoven, A. K. Nandakumaran, D. Roy, and R. M. Vasu (2011), A computationally efficient method for ultrasound-modulated optical tomography employing a weighted eigenvalue solution forthe forward problem, *Phy. Rev. E* **(Under Review)**.

[2] Hari M. Varma, Kuriyakkattil P. Mohanan, Nuutti Hyvnen, Akambadath K. Nandakumaran, and Ram M. Vasu (2011), Ultrasound-modulated optical tomography: recovery of amplitude of vibration in the insonified region from boundary measurement of light correlation, *J. Opt. Soc. Am. A* **28**, 2322–2311.

[3] S. Sakadzic and L. V. Wang (2006), Correlation transfer and diffusion of ultrasound-modulated multiply scattered light, *Phys. Rev. Lett.* **96**, 163902.

[4] B. J. Berne, R. Pecora (2000), *Dynamic Light Scattering*, Courier Dover Publications.

[5] A. Li, Q. Zhang, J. P. Culver, E. L. Miller, and D. A. Boas (2004), Reconstructing chromophore concentration images directly by continuous-wave diffuse optical tomography, *Opt. Lett.* **29**.

[6] H. K. Kim, M. Flexman, D. J. Yamashiro, J. J. Kandel, and A. H. Heilscher (2010), PDE-constrained multispectral imaging of tissue chromophores with the equation of radiative transfer, *Biomed. Opt. Express.* **1**, 812–824.

[7] E. Konofagou, J. Thierman, and K. Hynynen (2001), A focused ultrasound method for simulation, diagnostic and therapeutic applications: a simulation study, *Phys. Med. Biol.* **46**, 2967–2984.

[8] T. Kamakura, T. Ishiwata, and K. Matsuda (2001), Model equation for strongly focused finite-amplitude sound beams, *J. Opt. Soc. Am. A* **18**, 3035–3046.

[9] A. A.Oberai, N. H. Gokhale, and G. R. Feijoo (2003), Solution of inverse problems in elasticity imaging using the adjoint method, *Inverse Problems* **19**, 297–313.

[10] C. Usha Devi, R. M Vasu, and A. K. Sood (2005), Design, fabrication and characterization of tissue-equivalent phantoms for optical elastography, *J. Biomed. Opt.* **10**, 0440201 1–10.